ELSEVIER

Biochimica et Biophysica Acta 1524 (2000) 66–74

BIOCHIMICA ET BIOPHYSICA ACTA
BBA

www.elsevier.com/locate/bba

High resolution imaging of the distribution and permeability of methyl viologen dication in bovine articular cartilage using scanning electrochemical microscopy

Marylou Gonsalves [a], Julie V. Macpherson [a], Danny O'Hare [b], C. Peter Winlove [c], Patrick R. Unwin [a,*]

[a] *Department of Chemistry, University of Warwick, Coventry, CV4 7AL, UK*
[b] *Department of Pharmacy, University of Brighton, Brighton, BN2 4GJ, UK*
[c] *School of Physics, University of Exeter, Stocker Road, Exeter, EX4 4QL, UK*

Received 29 June 2000; received in revised form 14 September 2000; accepted 19 September 2000

Abstract

Scanning electrochemical microscopy (SECM) has been used in the induced transfer (SECMIT) mode to image the permeability of a probe cation, methyl viologen (MV^{2+}), in samples of articular cartilage. An ultramicroelectrode (UME), scanned just above the surface of a sample, is used to amperometrically detect the probe solute. The resulting depletion of MV^{2+} in solution induces the transfer of this cation from the sample into the solution for detection at the UME. The current provides quantitative information on local permeability, provided that the sample-UME distance is known. It is shown that the necessary topographical information can be obtained using the amperometric response for the oxidation of $Ru(CN)_6^{4-}$, which does not permeate into the cartilage matrix. This procedure was validated by marking samples in situ, after electrochemical imaging, with subsequent examination by ex situ interferometry and optical microscopy. Wide variations in the permeability of MV^{2+} have been detected by SECMIT. These observations represent the first demonstration of the inhomogeneous permeability of a cation in cartilage on a micrometre scale. The permeability maps show similar features to the proteoglycan distribution, identified by toluidine blue staining, and it is likely that proteoglycans are the main determinant of MV^{2+} permeability in articular cartilage.

Keywords: Scanning electrochemical microscopy; Ultramicroelectrode; Diffusion; Permeability; Cartilage; Proteoglycan

1. Introduction

Permeability is a key factor governing transport rates in biological membranes and tissues [1]. Articular cartilage is a specialised tissue for which permeability and fluid transport have been particularly well studied [2–5], due to the widespread belief that impaired mass transport is involved in diseases such as rheumatoid arthritis and osteoarthritis [6,7]. Cartilage comprises a porous supporting framework of collagen fibres, embedded in a gel composed of cells (chondrocytes), interstitial water and anionic proteoglycan molecules which confer a net negative fixed charge structure [8]. The exact proportion of each of the above components varies between joints, with depth within a joint and with age [9], and is altered by disease [10]. The largest variations are observed in the proportion of proteoglycans [2,11,12], which is of particular importance since these macromolecules influence significantly the transport of solutes and water through the cartilage matrix [13–16] as well as the viscoelastic properties of the tissue [17]. Some of the transport effects observed for small ions have been explained in terms of a microscopically inhomogeneous fixed negative charge distribution [14], but the experimental techniques available at the time lacked the spatial resolution to confirm this hypothesis.

The question of heterogeneity in transport has been addressed partially by taking advantage of the variations in tissue properties which occur with depth, to compare transport through tissue slices obtained at different depths within the tissue [3,14,15]. However, data were still averaged *across the surface of a slice*, thereby neglecting any lateral inhomogeneities in transport rates.

More recently, magnetic resonance imaging (MRI) has

* Corresponding author. Fax: +44 (24) 76524112;
E-mail: p.r.unwin@warwick.ac.uk

0304-4165/00/$ – see front matter
PII: S0304-4165(00)00142-2

emerged as a useful tool for the study of biological tissues such as cartilage [18]. A number of measurements of water and solute diffusion in cartilage have been reported [19–22]. The diffusivities of small singly charged anions and cations were found to be lower in cartilage than in free solution [19], in agreement with the findings of Maroudas [13]. Potter et al. [22] monitored the diffusion of the divalent cation, Cu^{2+}, in bovine nasal cartilage and found that the diffusion coefficient was inversely related to the fixed charge density of the tissue. The fixed charge density and proteoglycan distribution in cartilage have been mapped using MRI by investigating the electrostatic interaction of charged species, including Mn^{2+} [23], Na^{+} [24,25] and gadolinium diethylenetriaminepentaacetic acid [26,27], with the tissue matrix. Although MRI has the advantage of being non-invasive, with in vivo capabilities, the imaging resolution in complex tissues, such as cartilage, is limited by the low signal to noise ratio. An in plane resolution of 250–500 μm is typical [18], although higher resolutions (up to 26 μm [22]) have been reported for transport measurements.

Scanning electrochemical microscopy (SECM) is a powerful technique for examining the local transport of solutes by diffusion, convection and migration [28,29]. In SECM, a mobile ultramicroelectrode (UME) [30], positioned close to an interface with submicron precision, can be used to probe the topography, reactivity or permeability of that interface with high spatial resolution [31–33]. SECM has been applied to the study of a number of membranes and biomaterials including skin [34–39], dentine [40–42] and bilayer lipid membranes and cells [43–47]. In humid environments nanometre resolution is attainable, as evidenced by imaging studies of DNA [48]. SECM has the advantage over scanning ion conductance microscopy, which has found some application in the investigation of membrane transport [49,50], in that it can selectively detect both neutral and charged species, rather than measure total ion currents.

We have used SECM to image osmotically driven convective transport through laryngeal cartilage [51] and were able, for the first time, to correlate local convective fluxes with sample morphology on a microscopic scale. More recently, we have mapped localised oxygen permeability in bovine articular cartilage samples [52] using an SECM induced transfer (SECMIT) approach [53]. In SECMIT, the partitioning of a target solute between a bathing solution and a tissue sample is allowed to come to equilibrium. A UME, positioned in the bathing solution close to the sample surface, is biased at a potential to deplete the local concentration of solute at the tip via diffusion-limited electrolysis [52,53] or ion transfer [54]. This perturbs the equilibrium, driving the local transfer of solute from the tissue, thereby influencing the current flow to the UME probe. This approach allows measurements of diffusion, concentration or permeability of the solute in the tissue without the need to enter or contact the sample. This is particularly advantageous for measurements in biological tissues, where sample integrity is paramount. In our previous study, we were able to correlate spatially localised permeability with cellular topography, demonstrating that oxygen showed enhanced permeability in regions where cells were located, corresponding to areas where the distribution of collagen was most sparse.

In this paper, we report SECMIT studies aimed at quantitatively examining the permeability of a cationic species, methyl viologen (MV^{2+}), in articular cartilage. This choice of solute enables us to elucidate the interaction of cations with the negatively charged cartilage matrix. The quantitative application of SECMIT requires that the topography of the cartilage sample can be measured under the same conditions as the permeability measurements. This is achieved by carrying out hindered diffusion scans [55] with a negatively charged mediator which does not permeate into the cartilage matrix [52]. To validate this method, we have used a technique to mark the area of cartilage imaged by SECM for subsequent ex situ quantitative examination of surface topography using vertical scanning interferometry.

2. Materials and methods

2.1. Materials

Bovine articular cartilage, from the metacarpal phalangeal joints of mature animals, was obtained fresh from the abattoir and stored at −20°C prior to use. Full depth plugs of cartilage were removed from thawed joints using a 5 mm diameter cork borer and cut into 50 μm thick sections parallel to the articular surface on a microtome (Model 5030, Bright Instruments, Huntington, UK).

Before SECM experiments, the sections were equilibrated in a 0.2 mol dm^{-3} potassium chloride (KCl) (Analytical Reagent, Fisons, UK) solution, phosphate-buffered to pH 7.0 ± 0.2. SECM permeability imaging measurements were carried out with the cartilage sample bathed in a solution containing 5×10^{-3} mol dm^{-3} potassium hexacyanoruthenate (II) ($K_4Ru(CN)_6$) (Alfa, Royston, UK), 5×10^{-3} mol dm^{-3} methyl viologen dichloride hydrate ($MVCl_2$) (98%, Aldrich, UK) and 0.2 mol dm^{-3} KCl, phosphate-buffered to pH 7.0 ± 0.2. The solution was bubbled with nitrogen (oxygen free grade, BOC Gases, UK) for 30 min before pipetting gently into the SECM cell. During SECM imaging, a gentle stream of nitrogen was passed over the solution surface. This effectively excluded oxygen from the bathing solution, which would otherwise interfere with the electrochemical response for the reduction of MV^{2+} at the probe UME.

Samples were allowed to soak in the bathing solution for at least 1 h before measurements. Given the thinness of the samples, this was sufficient time for the system to equilibrate. The following solutions were used to mark

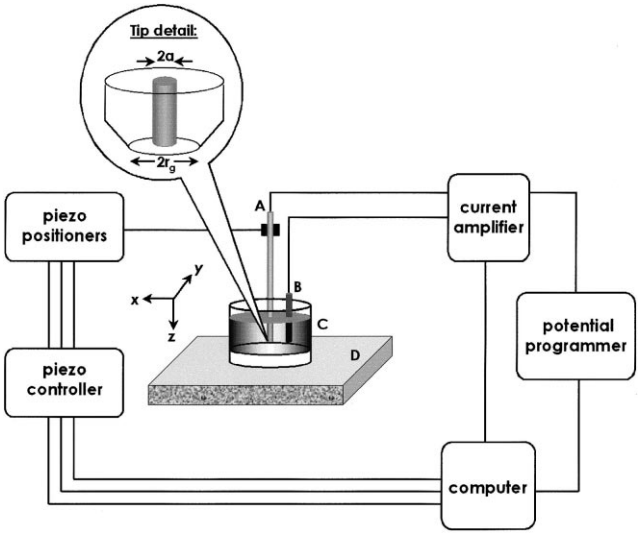

Fig. 1. Schematic (not to scale) of a typical SECM set up. A, UME; B, AgQRE; C, SECM cell with perspex body and PTFE base, on which sample is mounted; D, vibrationally isolated table.

the sample via localised Pd deposition: 1.0×10^{-2} mol dm^{-3} potassium tetrachloropalladate (K_2PdCl_4) (98%, Aldrich); followed by 1.0×10^{-2} mol dm^{-3} $MVCl_2$ in 0.2 mol dm^{-3} KCl. All solutions were prepared under ambient conditions, and measurements were made at room temperature (23 ± 1°C).

Representative cartilage sections were stained for histological analysis using standard protocols [56]: van Gieson's stain for collagen and toluidine blue for proteoglycans.

2.2. Instrumentation

The general SECM setup has been described previously [40], and is shown schematically in Fig. 1. A 5 μm diameter ($2a$) platinum disk electrode, embedded in a glass capillary, with an overall tip diameter, $2r_g$, of 50 μm was used for all measurements. The UME served as the working electrode in a conventional two-electrode setup, with a silver wire quasi-reference electrode (AgQRE), against which all potentials are quoted. The 50 μm thick cartilage sections were fixed on a glass disk using a procedure described previously [51,52]. The glass disk was then mounted in the base of an SECM cell so that the disk was perpendicular to the UME tip axis. The cell base also contained a draining hole to allow rinsing of the sample and changing of bathing solution without disturbing the position of the sample or UME.

Optical micrographs of samples were obtained using an Olympus BH2 microscope equipped with a 3-CCD colour video camera (model KY-F55BE, JVC Professional, London, UK) coupled to a computerised data acquisition system (Image Grabber/PCI, Neotech, London, UK).

Interferometry measurements were made on a WYKO NT2000 Optical Profiler (Veeco Instruments, UK) in vertical scanning interferometry (VSI) mode, using a white light source.

2.3. Procedures

2.3.1. SECM imaging

SECM images were obtained by holding the UME tip at a constant z position (normal to the interface) and scanning in the x-y plane (parallel to the interface) over an area of interest. When amperometrically detecting a solute to which the cartilage was impermeable, in this case $Ru(CN)_6^{4-}$, changes in the diffusion-limited current response, i, were due to variations in the sample-tip separation, d, from which topographical information on the sample surface could be obtained through the following relationship between $i/i(\infty)$ and d [57]:

$$i/i(\infty) = [0.292 + 1.515/(d/a) + 0.655\exp(-2.403/(d/a))]^{-1} \quad (1)$$

where $i(\infty)$ is the steady-state current with the tip positioned far from the sample.

When the same sample area was subsequently scanned, using a solute towards which cartilage was permeable, the current response was modified (as illustrated in Fig. 2), with the current now depending on both d and the permeability, defined as $K_e\gamma$, where $K_e = c_{cartilage}/c_{bathing\ solution}$ is the partition coefficient of the solute in cartilage. The term c_i denotes the solute concentration in the medium, i (cartilage or bathing solution). The term γ is the ratio of diffusion coefficients, D, of the solute in the two phases, $\gamma = D_{cartilage}/D_{bathing\ solution}$.

For the d and K_e values of interest in these studies, the relationship between $i/i(\infty)$, d and $K_e\gamma$ was determined numerically [52]. The following equation was found to best describe the numerical data for $0.05 \le K_e\gamma \le 0.95$ and 0.25 μm $\le d \le$ 7.05 μm (assuming a = 2.5 μm):

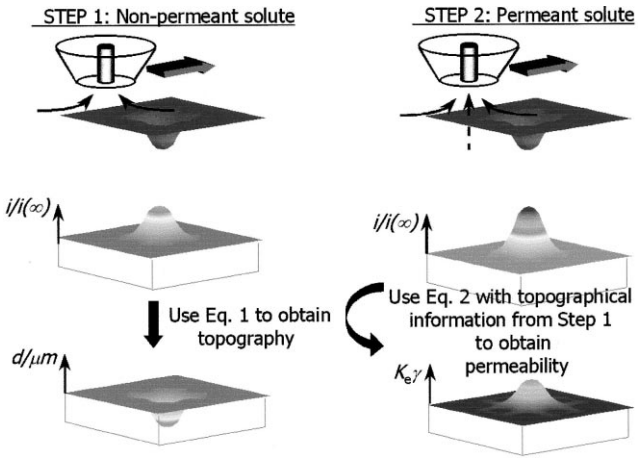

Fig. 2. Steps involved in making permeability measurements using SECMIT.

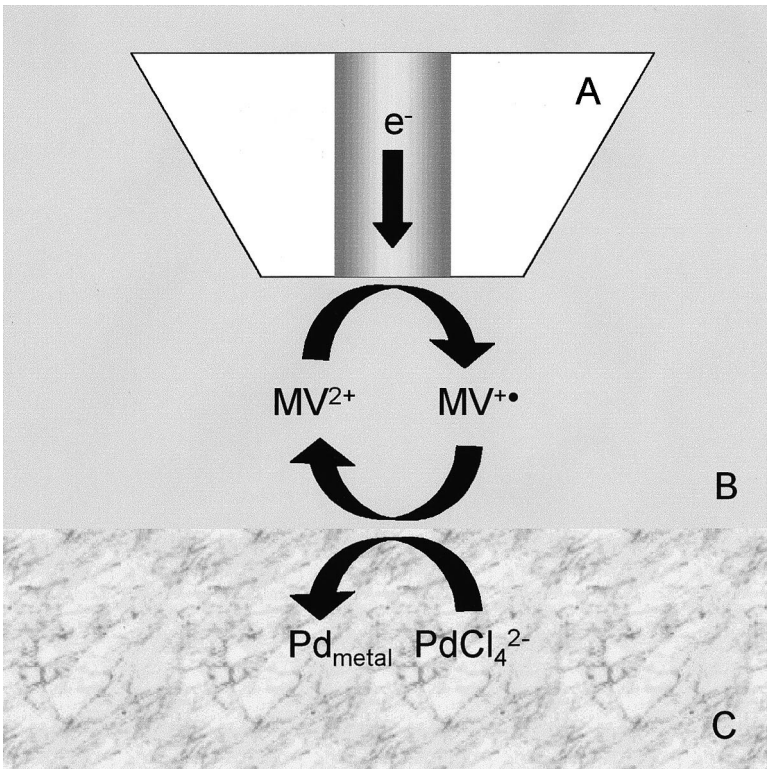

Fig. 3. Principles of the marking procedure by SECM feedback. (A) UME biased at −0.8 V to reduce MV^{2+}. (B) Solution containing MV^{2+}. (C) Cartilage tissue which has previously been soaked in $PdCl_4^{2-}$.

$$K_e\gamma = 2.1412-0.5885 \ln d-0.0002\times(1.0219\times10^8-2.1638\times10^7 \ln d + 7.0520\times10^6 \ln d^2-8.1320\times10^7 i/i(\infty))^{1/2} \quad (2)$$

To detect $Ru(CN)_6^{4-}$ by oxidation, the UME tip was biased at 1.2 V, where this process occurred at a diffusion-controlled rate. The value of $i(\infty)$ was measured, then the height of the tip above the cartilage sample was decreased until i attained a value of $0.25i(\infty)$. Based on the data herein, this corresponded to a sample-tip separation of approx. 1 μm [55]. The UME was then scanned laterally (in the x-y plane) over a 100 μm×100 μm area at 5 μm s^{-1} in unidirectional lines (101 points per line) with a separation of 5 μm between line scans, and i recorded as a function of lateral tip position. With these parameters, the spatial resolution of the technique, approx. 5 μm, is determined by the electrode diameter. At the end of the scan, the UME was retracted 200 μm from the cartilage surface and the value of $i(\infty)$ verified.

For MV^{2+} permeability scans, the tip was held at a potential of −0.8 V, to effect the diffusion-limited one-electron reduction of MV^{2+}. The UME was scanned over the same 100 μm×100 μm area as for the $Ru(CN)_6^{4-}$ map, with the same scan parameters, and the current ratio $i/i(\infty)$ determined. After imaging, the sample was marked using the method described below, to allow subsequent ex situ analysis by optical microscopy.

2.3.2. Sample marking for independent topography measurement

The areas of cartilage, imaged by SECM, were marked at their four corners using localised metal deposition on the sample surface via an SECM feedback technique [58] (illustrated schematically in Fig. 3). With the UME retracted 500 μm from the sample, the cell was drained and the sample and cell rinsed with copious amounts of water and soaked for 30 min in water to remove traces of $Ru(CN)_6^{4-}$. The sample was then rinsed again, and the cell drained, before soaking the sample in the $PdCl_4^{2-}$ solution. After 30 min, the sample was rinsed again with water. The sample retained an orange colour indicating the presence of $PdCl_4^{2-}$ in the matrix. The cell was then filled with MV^{2+} solution and the UME moved to the same height and co-ordinates (±0.1 μm) as used for the imaging experiments [59].

Over each corner of the scanned area, the UME was biased at −0.8 V, for 5 min, to reduce MV^{2+} in the vicinity of the electrode tip. This resulted in formation of $MV^{+\bullet}$, a strong reducing agent, which reduced $PdCl_4^{2-}$ in the tissue matrix to Pd metal at a localised spot on the surface. Designating the centre of the scanned area with the (x, y) co-ordinates (0 μm, 0 μm), the four corners corresponded to co-ordinates of, in order of marking, (−50 μm, −50 μm), (−50 μm, +50 μm), (+50 μm, +50 μm) and (+50 μm, −50 μm). To aid sample orientation on removal from the SECM cell, a fifth spot was marked

outside the scanned area at the (x, y) position (+50 μm, −100 μm).

For MV^{2+} permeability studies, the area imaged by SECM was marked at four corners outside the scanned area at (x, y) co-ordinates of (−75 μm, −75 μm), (−75 μm, +75 μm), (+75 μm, +75 μm) and (+75 μm, −75 μm), with the fifth mark at (+75 μm, −125 μm).

2.3.3. Interferometry measurements

The marked sample was first examined using optical microscopy, to check the visibility of the Pd spots. The sample was then transferred to the WYKO interferometry microscope, and the surface of the sample dried by gently wicking away excess solution with a lens tissue to remove the highly reflective surface solution which would otherwise prevent an accurate interferometry measurement. The sample was scanned in VSI mode over 20 μm in the z direction at a scan rate of 1 μm s^{-1}.

3. Results and discussion

The results presented in this paper are for two cartilage samples, but are typical of more than ten samples studied.

3.1. Cartilage topography

We previously suggested that $Ru(CN)_6^{4-}$ could be used as an SECM mediator to map the surface topography of cartilage samples, since this ion would be largely excluded from the matrix on electrostatic grounds [52]. Here, the aim was to confirm this quantitatively, by imaging selected areas of the cartilage matrix via $Ru(CN)_6^{4-}$ oxidation using SECM, and converting the current response to a topography map based on a hindered diffusion mass transport model (Eq. 1) [57]. The results obtained were then

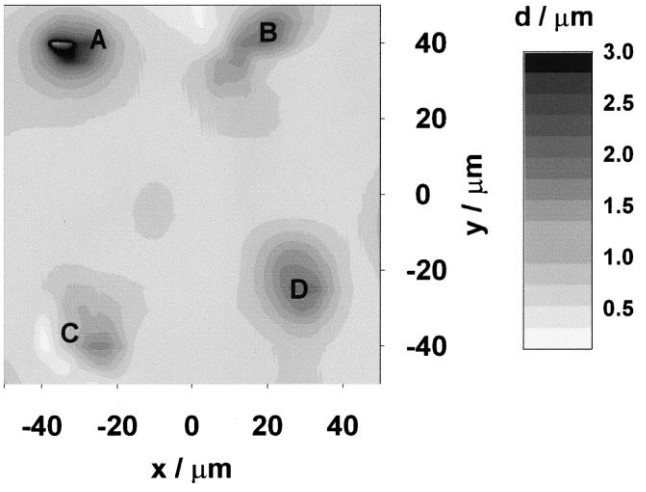

Fig. 4. Contour plot showing the sample topography of an area of cartilage imaged by diffusion-controlled oxidation of $Ru(CN)_6^{4-}$, with cellular features labelled A, B, C and D. Tip-sample separations (d) were calculated from oxidation current data using Eq. 1.

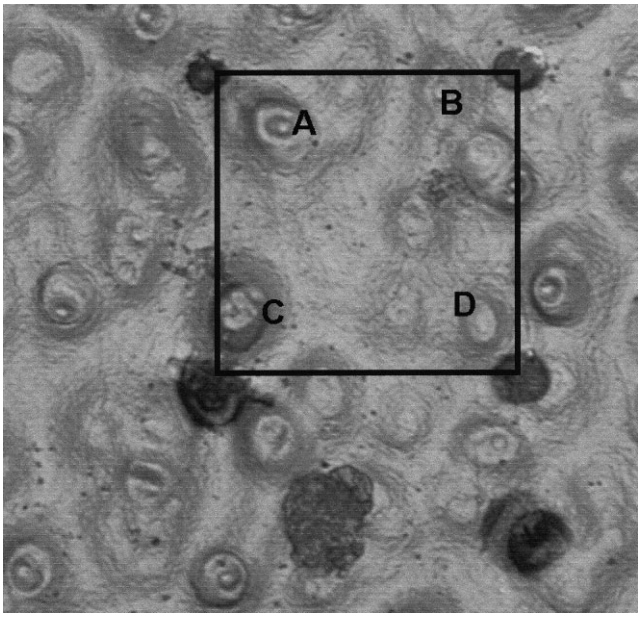

Fig. 5. Optical micrograph of the same area of cartilage imaged in Fig. 4, marked to indicate the scanned area. The superimposed square highlights the area imaged, with cellular features labelled A, B, C and D.

compared to an interferometric map of the same area of the sample, identified by marking via localised Pd deposition as discussed above.

Fig. 4 shows a contour plot of tip-substrate separation (surface topography) as a function of lateral tip position, calculated from current data for $Ru(CN)_6^{4-}$ oxidation using Eq. 1. It can be seen that there are circular recesses in the surface (labelled A to D), which we showed previously to correspond to regions where there had been cells or groups of cells within the surface of the cartilage slice [52]. From the SECM data, these recesses are 15–30 μm in diameter and approx. 3 μm deep.

An optical micrograph of the same area of the cartilage surface is shown in Fig. 5. The Pd deposits identifying the corners of the scanned area are clearly visible as black spots, with diameters ranging from 12 μm to 28 μm. The variation in the size of the Pd spots probably arises both from the different tip-substrate separations at the four corners of the scanned area, and the likely heterogeneous distribution of $PdCl_4^{2-}$ within the tissue matrix. An interferometry map of the marked area of cartilage is given in Fig. 6. A square outline (100 μm × 100 μm) has been superimposed to highlight the area that was scanned by SECM. When Figs. 4–6 are compared, we see that there is generally good agreement of the major topographical features in the surface of the sample (labelled A to D in all figures). Although the depths of some of the recesses measured by interferometry differ slightly from those obtained by SECM, this can be attributed to some dehydration of the sample in the interferometry measurements, resulting in a slight accentuation of the topographical features. Since it was necessary to dry the surface of the cartilage for the interferometry and light microscopy measurements,

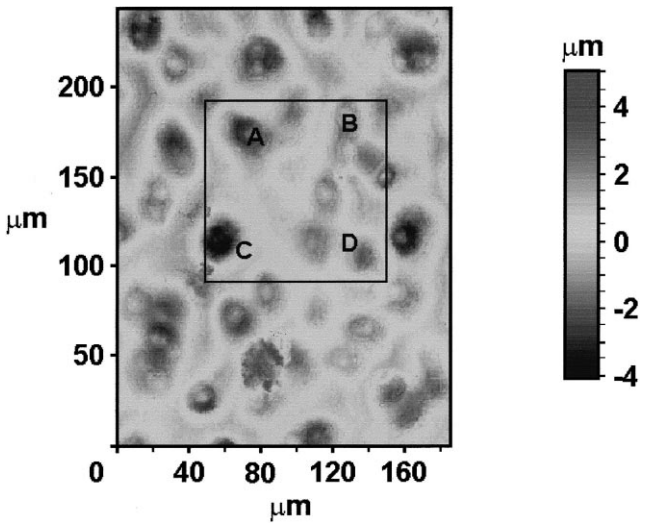

Fig. 6. Interferometry map of the same area of cartilage imaged in Fig. 4, marked to indicate the scanned area. The superimposed square highlights the area imaged, with cellular features labelled A, B, C and D.

we do not expect an exact correlation. Indeed there are some very shallow features in the interferometry measurement that are not detected by SECM. We consider this to be due to dehydration of the sample, since only relatively deep recesses (2–3 μm depth) have been observed in bathed cartilage samples by in situ AFM [52]. Nonetheless, apart from the slight discrepancies, these studies clearly demonstrate that the topography of a cartilage sample can be measured in situ by SECM, and that the cellular surface features observed agree well with those measured by interferometry.

3.2. MV^{2+} permeability

In order to determine the permeability of cartilage towards MV^{2+}, an area of the cartilage sample was first imaged with $Ru(CN)_6^{4-}$ to establish the sample topography. As the fixed charge of the cartilage matrix (as indicated by the location of proteoglycan macromolecules) varies greatly in the interterritorial region [12,52], an area of cartilage with few cellular features was located using this imaging procedure. Typical maps of normalised current vs. lateral tip position, and the corresponding tip-substrate separation vs. lateral tip position, are shown in Fig. 7. There is a circular region of enhanced current in Fig. 7a which appears as a recess of diameter approx. 30 μm and depth greater than 2 μm in the topography plot (Fig. 7b). The peripheries of other recesses are discernible at the top and bottom edges of the scanned area. The variation in topography over the remainder of the area imaged is of the order of 0.5 μm.

An optical micrograph of the scanned area is shown in Fig. 8, with two outlines superimposed indicating the

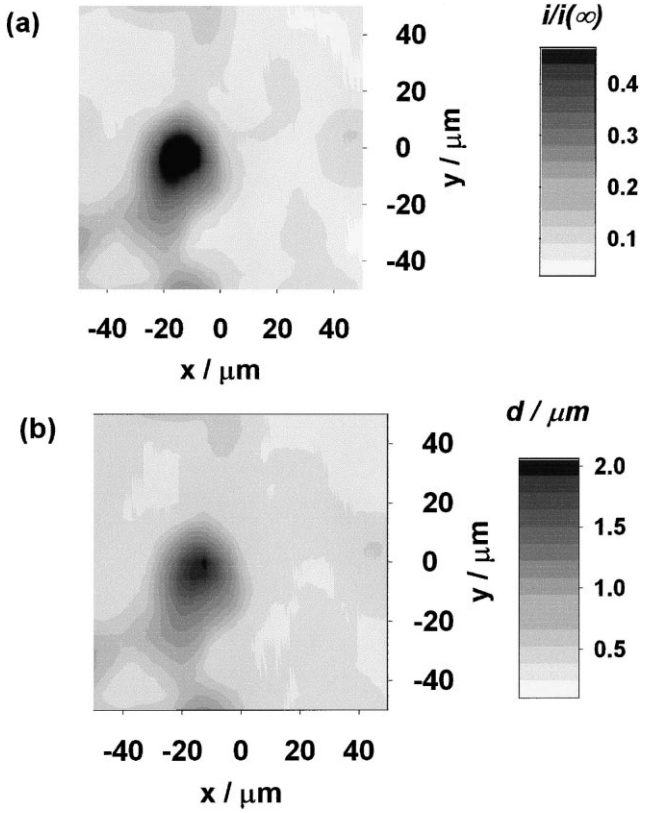

Fig. 7. Contour plots showing: (a) the normalised current map of an area of cartilage imaged by diffusion-controlled oxidation of $Ru(CN)_6^{4-}$, and (b) the corresponding topography map, calculated using Eq. 1.

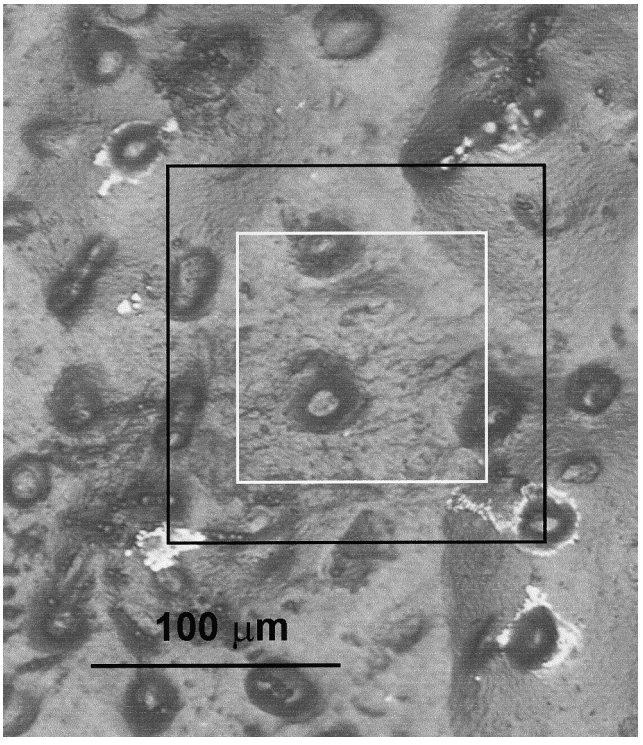

Fig. 8. Optical micrograph of the same area of cartilage imaged in Fig. 7, marked to indicate the scanned area. The superimposed squares highlight the marked (black) and scanned (white) areas.

marked area (black) and the scanned area (white). Excellent agreement is observed between the features in the micrograph and those seen in the SECM topography plot. In particular, a cellular recess with diameter 30 μm can be seen, which correlates well with the SECM topography scan.

Before obtaining the optical micrograph, and immediately after recording the $Ru(CN)_6^{4-}$ oxidation scan, the same area of cartilage was imaged via MV^{2+} reduction. As a cationic species, MV^{2+} in the aqueous solution is expected to interact with, and partition into, the negatively charged cartilage matrix. Fig. 9 shows a contour plot of normalised current as a function of lateral tip position. The normalised current response for this solute is very different to that for the topographical mediator, $Ru(CN)_6^{4-}$ (Fig. 7a). In general, all of the local currents are higher in Fig. 9, but there are also wider variations in the current response. In addition to the significantly enhanced current in the cellular region, there is considerable variation in current in the interterritorial region even though the surface topography plot and optical micrograph (Figs. 7b and 8, respectively) indicate that these areas are essentially flat.

As discussed in Section 2, we have previously shown that the permeability of a solute in a cartilage sample, defined as the product $K_e\gamma$, can be evaluated from the SECM current if the tip-substrate separation is known [52]. Using Eq. 2, the normalised current data for MV^{2+} reduction (Fig. 9) were analysed to take account of the varying tip-substrate separation (Fig. 7b), yielding a map of MV^{2+} permeability in the cartilage sample, shown in Fig. 10. The permeability of MV^{2+} is clearly heterogeneous over the scanned area, taking high values ($K_e\gamma$ up to 0.66) in the cellular region, while in the interterritorial region there is significant variation in $K_e\gamma$ between 0.1 and 0.4. This variation does not correlate simply with the surface morphology of the sample. If the diffusion

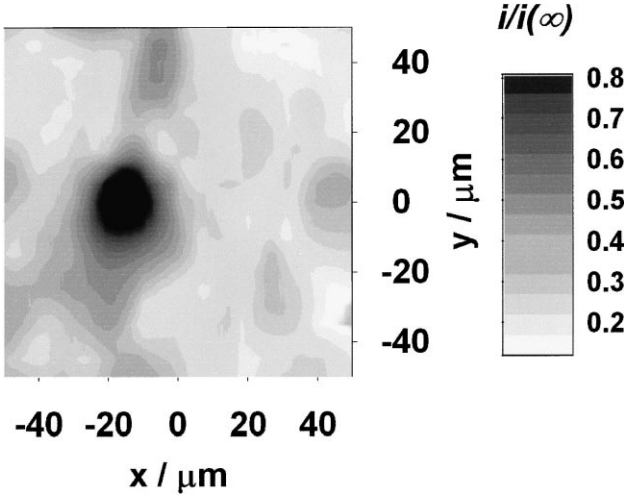

Fig. 9. Contour plot showing the normalised current map for the diffusion-controlled reduction of MV^{2+} over the same area of cartilage imaged in Fig. 7.

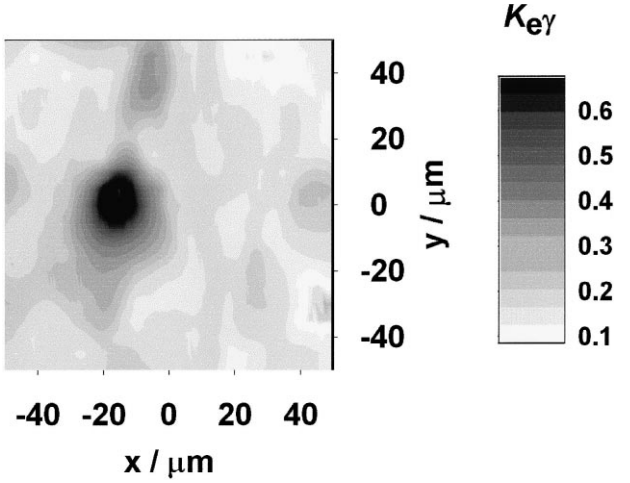

Fig. 10. Map of MV^{2+} permeability, $K_e\gamma$, calculated from the current data in Fig. 9, using Eq. 2.

coefficient does not vary appreciably, then the variation in permeability could be attributed to differences in K_e across the sample, i.e., variations in the distribution of MV^{2+} over the scanned area. Further work is, however, needed to confirm this hypothesis.

Cartilage sections, histologically stained to reveal the biochemical composition, are shown in Fig. 11a,b. It was necessary to use different cartilage sections to those imaged by SECM since $PdCl_4^{2-}$, required to mark the sample, interferes with the histological stains, particularly the stain for proteoglycans (toluidine blue) which relies on the charge of the proteoglycan macromolecules for effective staining. The staining for collagen (Fig. 11a) is lightest in the cellular region (where the nucleus is visible as a black spot), indicating a low distribution of collagen in this area. In the interterritorial region, the intensity of collagen staining is relatively uniform. The proteoglycan composition is quite different (Fig. 11b). There is intense staining around the periphery of the cells and the distribution in the interterritorial region shows considerable heterogeneity. Bearing these points in mind, examination of the permeability map indicates that the increased permeability of MV^{2+} in the cellular area occurs where the distribution of collagen, an important determinant of tissue permeability [60], is low. We have previously observed enhanced permeability of oxygen, an uncharged solute, in this area [52]. Considering the heterogeneous proteoglycan distribution in the interterritorial region, it is likely that the substantial variation in permeability of MV^{2+} arises through electrostatic interaction of this cation with the negatively charged proteoglycan molecules. If so, the higher permeability would be attributed to a higher density of proteoglycan molecules. Such interactions have been observed in cartilage under physiological conditions on a relatively large length scale [60]. However, this is the first time that wide variations in the permeability of a cation have been observed in cartilage at a micrometre level.

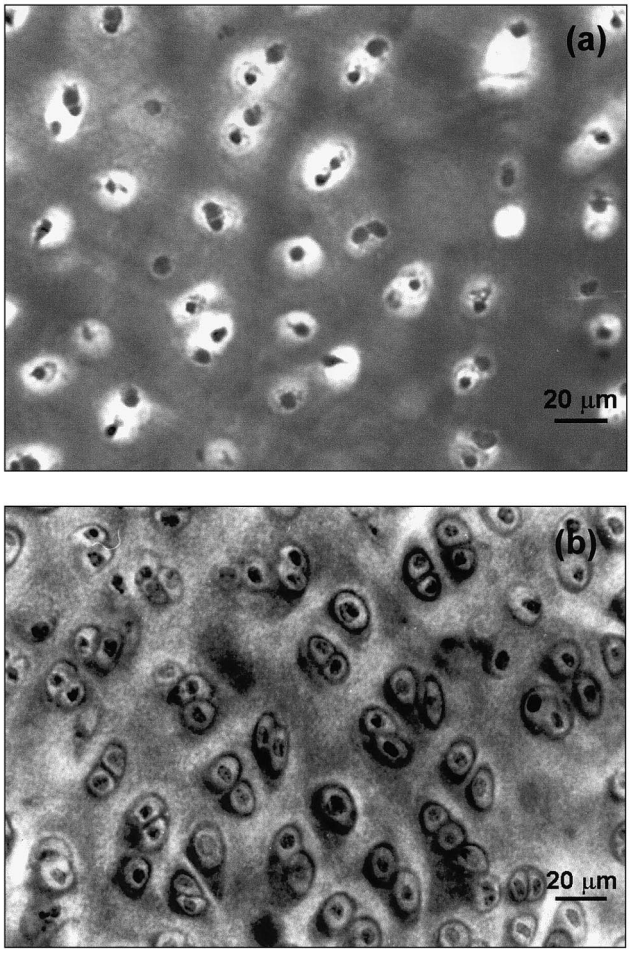

Fig. 11. Optical micrographs of histologically stained cartilage sections: (a) van Gieson's stain for collagen; (b) toluidine blue for proteoglycans.

4. Conclusions

We have demonstrated the use of SECMIT to map the permeability of MV^{2+} in cartilage with micrometre spatial resolution. Significant variations in permeability have been detected which are likely to correlate with the proteoglycan distribution in the exposed surface of the cartilage samples. In addition to the intrinsic interest in this new result, in terms of understanding the determinants of the permeability of small solutes in cartilage, the method could potentially be used as a means of imaging the proteoglycan distribution in cartilage. Further work in this direction is, however, needed to prove unequivocally a strict correlation between the electrochemical images and those obtained by conventional staining methods. This will require the development of a different procedure for marking the cartilage by SECM which does not interfere with the staining methods. The SECM methodology outlined in this paper could find ready application in imaging the permeability of solutes in a wide range of biomaterials. It should be straightforward to extend the method to viable tissue and living chondrocytes.

Acknowledgements

We thank Rosemary Ewins for preparation and histological staining of the samples. We gratefully acknowledge financial support from the Wellcome Trust (M.G., D.O'H., C.P.W. and P.R.U.) and the EPSRC (P.R.U. and J.V.M). J.V.M. also thanks the Royal Society for a University Research Fellowship. We are grateful to Prof. D.G. Chetwynd and Dr. V. Anghel (School of Engineering, University of Warwick) for their assistance with the interferometry measurements, and Miss A.L. Barker (Department of Chemistry, University of Warwick) for help with the SECMIT analysis.

References

[1] R. Fournier, Basic Transport Phenomena in Biomedical Engineering, Taylor and Francis, Philadelphia, PA, 1999.
[2] A. Maroudas, Biorheology 12 (1975) 233.
[3] E. Bernich, R. Rubenstein, J.S. Bellin, Biochim. Biophys. Acta 448 (1976) 551.
[4] R.V. Allhands, P.A. Torzilli, F.A. Kallfelz, Cornell Vet. 74 (1984) 111.
[5] V.C. Mow, M.H. Holmes, W.M. Lai, J. Biomech. 17 (1984) 377.
[6] K.E. Keuttner, R. Schleyerbach, J.G. Peyron, V.C. Hascall (Eds.), Articular Cartilage and Osteoarthritis, Raven Press, New York, 1992.
[7] C. Muehleman, C.H. Arsenis, J. Am. Podiatr. Med. Assoc. 85 (1995) 282.
[8] N.G. Shrive, C.B. Frank, in: B. Nigg and W. Herzog (Eds.), Biomechanics of the Musculo-Skeletal System, J. Wiley and Sons, Chichester, 1994, pp. 79–105.
[9] M.F. Venn, Ann. Rheum. Dis. 37 (1978) 168.
[10] M. Venn, A. Maroudas, Ann. Rheum. Dis. 36 (1977) 121.
[11] R. Lemperg, S.-E. Larsson, Calcif. Tissue Res. 15 (1974) 237.
[12] P.J. Roughley, E.R. Lee, Microsc. Res. Tech. 28 (1994) 385.
[13] A. Maroudas, Biophys. J. 8 (1968) 575.
[14] A. Maroudas, Biophys. J. 10 (1970) 365.
[15] P.A. Torzilli, J.M. Arduino, J.D. Gregory, M. Bansal, J. Biomech. 30 (1997) 895.
[16] S. Roberts, J.P.G. Urban, H. Evans, S.M. Eisenstein, Spine 21 (1996) 415.
[17] M.B. Schmidt, V.C. Mow, L.E. Chun, D.R. Eyre, J. Orthop. Res. 8 (1990) 353.
[18] L.R. Frank, E.C. Wong, R.B. Buxton, D.R. Resnick, Top. Magn. Reson. Imaging 10 (1999) 153.
[19] D. Burstein, M.L. Gray, A.L. Hartman, R. Gipe, B.D. Foy, J. Orthop. Res. 11 (1993) 465.
[20] A.E. Fischer, T.A. Carpenter, J.A. Tyler, L.D. Hall, Magn. Reson. Imaging 13 (1995) 819.
[21] R. Knauss, G. Fleischer, W. Grunder, J. Kärger, A. Werner, Magn. Reson. Med. 36 (1996) 241.
[22] K. Potter, R.G.S. Spencer, E.W. McFarland, Biochim. Biophys. Acta 1334 (1997) 129.
[23] Y. Kusaka, W. Grunder, H. Rumpel, K.-H. Dannhauer, K. Gersonde, Magn. Reson. Med. 24 (1992) 137.
[24] L.M. Esperance, M.L. Gray, D. Burstein, J. Orthop. Res. 10 (1992) 1.
[25] E.M. Shapiro, A. Borthakur, R. Dandora, A. Kriss, J.S. Leigh, R. Reddy, J. Magn. Reson. 142 (2000) 24.
[26] A. Bashir, M.L. Gray, J. Hartke, D. Burstein, Magn. Reson. Med. 41 (1999) 857.
[27] S. Trattnig, V. Mlynárik, M. Breitenseher, M. Huber, A. Zembsch, T. Rand, H. Imhof, Magn. Reson. Imaging 17 (1999) 577.

[28] A.J. Bard, F.-R.F. Fan, D.T. Pierce, P.R. Unwin, D.O. Wipf, F. Zhou, Science 254 (1991) 68.
[29] J.V. Macpherson, P.R. Unwin, Chem. Ind. (1995) 874.
[30] R.M. Wightman, D.O. Wipf, in: A.J. Bard (Ed.), Electroanalytical Chemistry, vol. 15, Marcel Dekker, New York, 1989, pp. 267–353.
[31] A.J. Bard, F.-R.F. Fan, M.V. Mirkin, in: A.J. Bard (Ed.), Electroanalytical Chemistry, vol. 18, Marcel Dekker, New York, 1994, pp. 243–373.
[32] A.L. Barker, M. Gonsalves, J.V. Macpherson, C.J. Slevin, P.R. Unwin, Anal. Chim. Acta 385 (1999) 223.
[33] M.V. Mirkin, B.R. Horrocks, Anal. Chim. Acta 406 (2000) 119.
[34] B.D. Bath, R.D. Lee, H.S. White, E.R. Scott, Anal. Chem. 70 (1998) 1047.
[35] B.D. Bath, H.S. White, Anal. Chem. 72 (2000) 433.
[36] E.R. Scott, H.S. White, J.B. Phipps, J. Membr. Sci. 58 (1991) 71.
[37] E.R. Scott, A.I. Laplaza, H.S. White, J.B. Phipps, Pharm. Res. 10 (1993) 1699.
[38] E.R. Scott, H.S. White, J.B. Phipps, Anal. Chem. 65 (1993) 1537.
[39] E.R. Scott, J.B. Phipps, H.S. White, J. Invest. Dermatol. 104 (1995) 142.
[40] J.V. Macpherson, M.A. Beeston, P.R. Unwin, N.P. Hughes, D. Littlewood, J. Chem. Soc. Faraday Trans. 91 (1995) 1407.
[41] J.V. Macpherson, M.A. Beeston, P.R. Unwin, N.P. Hughes, D. Littlewood, Langmuir 11 (1995) 3959.
[42] P.R. Unwin, J.V. Macpherson, M.A. Beeston, N.J. Evans, N.P. Hughes, D. Littlewood, Adv. Dent. Res. 11 (1997) 548.
[43] T. Matsue, H. Shiku, H. Yamada, I. Uchida, J. Phys. Chem. 98 (1994) 11001.
[44] T. Yasukawa, I. Uchida, T. Matsue, Biochim. Biophys. Acta 1369 (1998) 152.
[45] T. Yasukawa, T. Kaya, T. Matsue, Anal. Chem. 71 (1999) 4637.
[46] T. Yasukawa, I. Uchida, T. Matsue, Biophys. J. 76 (1999) 1129.
[47] M. Tsionsky, J.F. Zhou, S. Amemiya, F.-R.F. Fan, A.J. Bard, R.A.W. Dryfe, Anal. Chem. 71 (1999) 4300.
[48] F.-R.F. Fan, A.J. Bard, Proc. Natl. Acad. Sci. USA 96 (1999) 14222.
[49] P.K. Hansma, B. Drake, O. Marti, S.A.C. Gould, C.B. Prater, Science 243 (1989) 641.
[50] Y.E. Korchev, C.L. Bashford, M. Milovanovic, I. Vodyanoy, M.J. Lab, Biophys. J. 73 (1997) 653.
[51] J.V. Macpherson, D. O'Hare, P.R. Unwin, C.P. Winlove, Biophys. J. 73 (1997) 2771.
[52] M. Gonsalves, A.L. Barker, J.V. Macpherson, P.R. Unwin, D. O'Hare, C.P. Winlove, Biophys. J. 78 (2000) 1578.
[53] A.L. Barker, J.V. Macpherson, C.J. Slevin, P.R. Unwin, J. Phys. Chem. B 102 (1998) 1586.
[54] N.J. Evans, M. Gonsalves, N.J. Gray, A.L. Barker, J.V. Macpherson, P.R. Unwin, Electrochem. Commun. 2 (2000) 201.
[55] J. Kwak, A.J. Bard, Anal. Chem. 61 (1989) 1221.
[56] H.M. Carleton, Carleton's Histological Technique, Oxford University Press, Oxford, 1980.
[57] M.V. Mirkin, F.-R.F. Fan, A.J. Bard, J. Electroanal. Chem. 328 (1992) 47.
[58] D. Mandler, A.J. Bard, J. Electrochem. Soc. 137 (1990) 1079.
[59] J.V. Macpherson, P.R. Unwin, J. Phys. Chem. 99 (1995) 3338.
[60] P.M. Gribbon, A. Maroudas, K.H. Parker, C.P. Winlove, in: R.K. Reed, K. Rubin (Eds.), Connective Tissue Biology. Integration and Reductionism, Portland Press, London, 1998, pp. 95–123.